AIChE Journal
DOI10.1002/aic.16299

# Gas–liquid–solid reaction system for $CO_2$ electroreduction to formate without using supporting electrolyte

Guillermo Díaz-Sainz[1,*], Manuel Alvarez-Guerra[1], José Solla-Gullón[2], Leticia García-Cruz[2], Vicente Montiel[2], Angel Irabien[1]

[1]Chemical and Biomolecular Engineering Department, University of Cantabria, ETSIIT, Avda. Los Castros s/n 39005, Santander, Spain

[2]Institute of Electrochemistry, University of Alicante, Apdo. 99, E-03080 Alicante, Spain

*Corresponding author: diazsg@unican.es

## Abstract

The use of bismuth-based catalysts is promising for formate production by the electroreduction of $CO_2$ captured from waste streams. However, compared to the extensive research on catalysts, only a few studies have focused on electrochemical reactor performance. Hence, this work studied a continuous-mode gas–liquid–solid reaction system for investigating $CO_2$ electroreduction to formate using Bi-catalyst-coated membrane electrodes as cathodes. The experimental setup was designed to analyze products obtained in both liquid and gas phases. The influence of relevant variables (e.g.,


Received: Nov 15, 2019;Revised: May 20, 2020;Accepted: Jun 10, 2020

temperature and input water flow) was analyzed, with the thickness of the liquid film formed over the cathode surface being a key parameter affecting system performance. Promising results, including a high formate concentration of 34 $g \cdot L^{-1}$ with Faradaic efficiency for formate of 72%, were achieved.

**Keywords:** $CO_2$ electroreduction, Bismuth, Formate, CCMEs (catalyst-coated membrane electrodes), G–L–S reaction system

## Introduction

One of the most important challenges we are faced with as a global community is climate change mitigation. According to the Paris Climate Conference (COP21), limiting the temperature increase to below 2.0 ºC and pursuing efforts to limit it to 1.5 ºC will be crucial to diminish the risks and the consequences of climate change [1]. Moreover, the primary contributors to global climate change are greenhouse gases such as carbon dioxide ($CO_2$), methane ($CH_4$), nitrous oxide, and fluorinated gases (chlorofluorocarbons, hydrochlorofluorocarbons, and halons) [2]. $CO_2$ is the main greenhouse gas released through anthropogenic activities, so reducing anthropogenic $CO_2$ emissions into the atmosphere should be a priority in order to mitigate climate change [3].

Different approaches have been considered to lower $CO_2$ emissions [4]. Improving energy efficiency or fuel switching to renewable sources of energy is one of the most common alternatives to reduce $CO_2$ emissions [5]. However, recent studies based on carbon capture and sequestration (CCS) and carbon capture and utilization (CCU) show the promise of

these technologies in reducing $CO_2$ emissions [6]. In particular, the valorization of $CO_2$ into useful products has been highlighted as a promising strategy, because it mitigates $CO_2$ emissions and, concurrently, converts $CO_2$ into value-added chemicals [7–9].

In fact, $CO_2$ can be converted into useful products through various routes, such as thermochemical or mineralization processes [10], photochemical reduction [11] or electrochemical reduction [12]. Among these options, the electrocatalytic reduction of $CO_2$ into useful chemicals has been considered as a promising strategy for CCU because it would allow the storage of excess renewable and intermittent sources of energy into value-added chemical products, which could be utilized to produce fuels [13–15].

In this context, different chemical products can be obtained by the electrochemical reduction of $CO_2$ depending on different aspects, for example, the catalytic material used, the reaction medium used, or the voltage applied in the electrochemical process, among others [16]. The possible products that can be obtained by $CO_2$ electroreduction include formic acid (HCOOH) [17], carbon monoxide (CO) [18], and hydrocarbons or alcohols [19].

Formic acid or formate ($HCOO^-$), depending on pH, can be used in various industries [17]. Moreover, this chemical has been proposed as a fuel for low-temperature fuel cells [20] and as a hydrogen carrier [21]. According to previous studies, different electrocatalysts and systems with a filter-press electrochemical cell have been used in the electroconversion of $CO_2$ to obtain $HCOO^-$. Sn has been widely studied as a catalyst in $CO_2$ electroreduction to $HCOO^-$ [22–29]. However, other electrocatalysts have also been tested for $CO_2$ conversion to obtain $HCOO^-$, such as Pb [30–32], In [33,34], Pd [35,36], and Bi [37–43], which are less common.

Bi could be an effective alternative to Sn owing to the lower potentials required in the electrochemical reactor with respect to other electrocatalysts [44–46].

Compared to the vast amount of research on catalysts, few studies have focused on the electrochemical reactor, as has recently been highlighted by Vennekoetter et al. 2019 [47]. The previous work of our research group studied the use of Pb, Sn, and Bi in the $CO_2$ electroconversion to $HCOO^-$ in various systems with a filter-press electrochemical reactor. Metal plates were initially used as working electrodes in the electrochemical conversion of $CO_2$ to obtain $HCOO^-$ [32,48]. Gas diffusion electrodes (GDEs) have also been developed, in which the electrocatalyst is deposited over a carbonaceous support [49–51]. In fact, in both configurations of working electrodes (i.e., metal plates and GDEs), the $CO_2$-saturated catholyte stream is fed to the electrochemical reactor for $CO_2$ electroreduction to $HCOO^-$. In the GDE configuration, the additional supply of $CO_2$ in an input gaseous stream allows the reaction to occur in a three-phase boundary gas–liquid–solid (G–L–S). The system is limited because of the low $CO_2$ concentration in the liquid electrolyte, the effects of diluting the products in the liquid electrolyte and the costs associated with the subsequent separation process of the liquid product from the electrolyte.

Accordingly, some recent studies from our research group [52] have focused on the development of $CO_2$ gas-phase electroconversion to produce formate through the use of Sn-catalyst-coated membrane electrodes (Sn-CCMEs), avoiding the use of a liquid electrolyte in order to improve the $CO_2$ solubility and the cost attributed to the separation process. First, a humidified $CO_2$ stream is fed to the electrochemical reactor instead of introducing the $CO_2$-saturated liquid electrolyte stream. Moreover, the fabrication

methodology of the working electrode is different from that of GDEs, with the electrocatalyst deposited directly over the Nafion 117 membrane instead of depositing it over the carbonaceous support. Hence, a humidified $CO_2$ gas stream improves the delivery of gaseous $CO_2$ to the G–L–S interface, avoiding the use of a liquid electrolyte and therefore, the $CO_2$ solubility limitation in the electrolyte. The Nafion 117 membrane acts as a solid polymer electrolyte and as a support for the catalytic material. Nevertheless, the performance of this type of reaction system has rarely been studied in the $CO_2$ electroconversion to give formate using Bi as the catalyst, while working in a continuous mode with a single pass of the saturated $CO_2$ stream with $H_2O$ in a filter-press electrochemical reactor.

This work studies the electrochemical reduction of $CO_2$ to produce formate using Bi carbon-supported nanoparticles (Bi/C NPs) as catalysts in the form of CCMEs (Bi/C-CCMEs) within a G–L–S electrochemical reaction system, operating in a continuous mode with a single pass of $CO_2$ humidified stream through the reactor. Moreover, some important key variables have been studied, such as temperature, water flow in the $CO_2$ stream, current density (*J*), and Bi catalyst loading (*CL*), in order to assess the performance of the electrochemical G–L–S reaction, which has only been reported in a few previous studies[23,52] on $CO_2$ electrovalorization to obtain formate. Although this study focuses on obtaining formate as the main product, both liquid and gas phases were analyzed in order to detect and quantify other byproducts that could be obtained in the $CO_2$ electroreduction process using Bi/C-CCMEs.

## Methodology

### Fabrication of Bi/C-CCMEs

To prepare Bi/C-CCMEs, carbon-supported Bi nanoparticles (9–10 nm) (Bi/C NPs) were prepared using a methodology described in previous studies [53]. An airbrushing technique was used to fabricate Bi/C-CCMEs, as shown in Figure 1. First, the catalytic ink was prepared by mixing Bi/C NPs and a certain amount of Nafion (Nafion D-521 dispersion, 5% w/w in water and 1-propanol, ≥0.92 meq/g exchange capacity, Alfa Aesar) in a ratio of 70:30 and diluted in isopropanol (isopropanol, 99.5%, Extra Dry over Molecular Sieve, AcroSeal®) in a final solution of 3 wt.% of catalyst/Nafion in isopropanol.

**Figure 1.** Schematic of the airbrushing technique used to fabricate Bi/C-CCMEs.

Consequently, the catalytic ink was sonicated for 30 min and then sprayed over the Nafion 117 membrane, which had a geometric surface area of 10 $cm^2$. The Nafion 117 membrane was placed over a hot metallic plate set to a temperature of 60–70 ºC in order to improve isopropanol evaporation. Different Bi *CL*s—0.75 and 1.5 $mg \cdot cm^{-2}$—were used.

### Characterization of Bi/C-CCMEs

Field emission scanning electron microscopy (FESEM, ZEISS Merlin VP Compact microscope with an X-ray detector BRUKER Quantax 400 for EDX microanalysis and mapping) was employed to analyze the morphology and Bi distribution of the CCMEs.

**Filter-press cells and experimental conditions**

Figure 2 depicts the experimental setup for the electrocatalytic reduction of $CO_2$ to obtain $HCOO^-$ in a filter-press electrochemical reactor (Micro Flow Cell, ElectroCell A/S) using Bi/C-CCME as the working electrode.

**Figure 2.** Experimental setup used for the tests of Bi/C-CCMEs for the study of $CO_2$ electrochemical reduction to obtain $HCOO^-$: 1 (Peristaltic pump); 2 (Filter press reactor); 3 (Vapor Delivery Module); 4 (Potentiostat-galvanostat); 5 (G/L Separator); 6 (Filters); 7 (Trap); 8 (Ion chromatography); 9 (Gas chromatography).

As illustrated in Figure 3, the Bi/C-CCME acts as a cathode and simultaneously acts as a separator between the anode and cathode compartments. At the cathode side, a humidified $CO_2$ stream was fed to the working electrode compartment of the electrochemical reactor, and a tinned steel mesh was used as the current collector. Moreover, the water flow in the $CO_2$ stream and the temperature were controlled by a vapor delivery module. These variables were also measured in the output stream of the electrochemical reactor using a HygroFlex HF5 humidity temperature transmitter. At the anode side, a commercial dimensionally stable anode [DSA/$O_2$ (Ir-MMO (mixed metal oxide) on platinum), Electrocell] was used in the electrochemical filter-press reactor. On the one hand, the metal mix of the counter electrode is composed by both Ti and Ir oxides. In contrast, the Ir loading in the mix was 16 $g \cdot m^{-2}$. In addition, a 1 M KOH (potassium hydroxide, 85%

purity, pharma grade, PanReac AppliChem) aqueous solution was used as the anolyte with a flow of 5.7 $mL \cdot min^{-1}$.

**Figure 3.** Electrochemical filter-press reactor configuration for the tests of Bi/C-CCMEs used for the continuous electroreduction of $CO_2$ to obtain $HCOO^-$.

The experimental setup was developed to allow the analysis of both liquid and gas phases, instead of only analyzing the liquid phase, as in our previous studies [52]. The gas phase was analyzed using a 4-channel micro gas chromatograph (490, Micro GC, Agilent Technologies) equipped with a thermal conductivity detector (Micro-TCD). Helium and argon (99.99% purity) were employed as the carrier gases. Hydrogen ($H_2$), nitrogen ($N_2$), oxygen ($O_2$), CO, $CH_4$ and noble gases were separated in a molecular sieve 5 Å column (10 m MS5A Hi-BF SP1 pre-column), whereas $CO_2$ and long-chain hydrocarbons were separated in a PoraPLOT U PLO mm ID column (10 m PPU HI-BF). Volatile solvents and polar compounds were also measured using a CP-Sil 5 CB, 015 mm ID (8 m, 5CB HI-Str) and an SP1 column (10 m, 52 CB HI-Str), respectively. Moreover, the liquid phase was analyzed using an ion chromatograph (Dionex ICS 1100) equipped with an AS9-HC column and a headspace gas chromatograph (GCMSQP2010 Ultra Shimadzu) equipped with a flame ionization detector. The experiments had a duration of 90 min. Samples were taken every 30 min to analyze both the liquid and gas phases, and the average value of the concentrations of each detected product was obtained for each experiment. Moreover, all experiments were performed in duplicate under the same operating conditions, ensuring the maximum standard deviations for the replicates of each experimental point were lower than 10% of the average concentration of each product.

The performance of the electrochemical process is assessed by the Faradaic efficiency and the concentration of each product as well as the rate and consumption of energy of $HCOO^-$. The different equations used to calculate these performance criteria can be found in literature [52].

## Results and Discussion

### Characterization of Bi/C-CCMEs

Figure S1 of the Supporting Information shows the representative SEM images (surface and cross section) of the Bi/C-CCMEs, including some EDX Bi mapping profiles. The SEM-EDX results show that the Bi electrocatalyst is well-dispersed and homogeneously distributed over the surface of the electrode. The thickness of the catalytic layer is approximately 15–20 μm.

### Performance of the G–L–S continuous reaction system

#### Temperature

Various tests were carried out to analyze the influence of temperature on the performance of the reaction system. All experiments were carried out in a continuous mode with only one pass of the input stream through the electrochemical reactor. In this subsection, all tests were performed at a current density ($J$) of 45 $mA \cdot cm^{-2}$ with a Bi $CL$ of 0.75 $mg \cdot cm^{-2}$.

For each experiment, both the liquid and gas phases were analyzed in duplicate to determine the Faradaic efficiency (*FE*) and rate (*r*) for each product. Formate is the main product detected in the liquid phase using ion chromatography, with traces of methanol ($CH_3OH$) and ethanol ($C_2H_5OH$) determined by headspace gas chromatography. Thus, the formate concentration (*[HCOO$^-$]*) and the consumption of energy per kilogram of formate (*EC*) are calculated.

Experiments were performed between 293 K and 323 K, with intermediate temperature values of 298 K and 310.5 K. The experiments were performed with a constant relative humidity in the $CO_2$ stream of 100%. Figure 4 summarizes the results regarding formate production in the liquid phase. On the one hand, Figure 4a represents the variation of formate rate ($r_F$) and the Faradaic efficiency for formate ($FE_F$) for different values of temperature tested. In contrast, Figure 4b shows the influence of temperature on *[HCOO$^-$]* and the *EC* needed to produce formate.

**Figure 4.** Influence of temperature on (a) formate rate (mmol·m$^{-2}$·s$^{-1}$) and Faradaic efficiency for formate (%) and (b) the consumption of energy per kmol of formate (MJ·kmol$^{-1}$) and Formate concentration (g·L$^{-1}$) in the temperature range of 293–323 K applied at constant current density = 45 mA·cm$^{-2}$, Bi CL = 0.75 mg·cm$^{-2}$, and relative humidity = 100%.

As can be seen in Figure 4a, at a temperature of 293 K, $r_F$ of 1.10 mmol·m$^{-2}$·s$^{-1}$ is obtained. However, increasing the temperature of the saturated $CO_2$ stream in the input of the electrochemical reactor from 293 K to 298 K, the $r_F$ drops to 1.08 mmol·m$^{-2}$·s$^{-1}$. This variation in $r_F$ can be attributed to the standard deviation (SD) of the experiments (SD values are reported in Table S1 of the Supporting Information). Nevertheless, after

increasing the temperature to 323 K, $r_F$ and $FE_F$ decrease by approximately 14.5% compared to room temperature. Although Lee et al. 2018[23] reported a different trend in the influence of temperature, these results are in agreement with those previously reported in literature, where working at 293 K represents the optimal operating temperature [54], which could be attributed to the fact that the solubility of $CO_2$ in the liquid layer of water formed in the G–L–S reaction system decreases with increasing temperature.

Figure 4b shows that the highest *[HCOO$^-$]* obtained was at a temperature of 293 K (22.3 g·L$^{-1}$). Moreover, by performing the electrochemical process at 293 K, the lowest value of *EC* per kmol of formate is also reached, which is approximately 1123.2 MJ·kmol$^{-1}$. On the one hand, increasing the temperature of the input $CO_2$ stream to 313 K, the *[HCOO$^-$]* decreases by approximately 21%, from 22.3 to 17.6 g·L$^{-1}$. The $CO_2$ stream in the electrochemical filter-press reactor was fed as a saturated stream with $H_2O$; therefore, the higher temperature led to an increase in the amount of water in the $CO_2$ stream in order to achieve saturation in the $CO_2$ stream. Increasing the water flow in the $CO_2$ stream may be directly related to the performance in the filter-press reactor, which is closer to that corresponding to a liquid electrolyte instead of a solid polymer electrolyte. In contrast, operating at a temperature of 313 K increases the *EC* to give formate by approximately 30%, from 1123.2 to 1465.2 MJ·kmol$^{-1}$, which is higher than operating at room temperature.

Both the liquid and gas phases were analyzed in order to determine the product distribution over the temperature range of 293–323 K. The results are summarized in Figure 5 (values are described in Table S2 in the Supporting Information). In addition to

$HCOO^-$ in the liquid phase, $H_2$, CO, $CH_4$, and ethylene ($C_2H_4$) were detected as gaseous products. It should be noted that the accumulated $FE_F$, the Faradaic efficiency for $H_2$ ($FE_H$), the Faradaic efficiency for CO ($FE_C$), the Faradaic efficiency for $CH_4$ ($FE_C$) and the Faradaic efficiency for $C_2H_4$ ($FE_C$) values of these products were close to 100%. As shown in Figure 5, increasing the temperature from 293 K to 323 K results in a lower $FE_F$. This decrease is mostly due to the hydrogen evolution reaction, which is favored as the temperature increases [55]. The highest $FE_H$ value (50.9%) was obtained at an operating temperature of 323 K, which is 26% higher than that obtained at room temperature (40.2%). However, $FE_C$ and $FE_M$ were almost constant at 10 and 2.5% at 293–313 K, respectively. Furthermore, small traces of $C_2H_4$ appeared at operating temperatures of 310.5 and 323 K in the $CO_2$ saturated stream with $H_2O$.

**Figure 5.** Influence of temperature on the *FE* of formate ($FE_F$), hydrogen ($FE_H$), carbon monoxide ($FE_C$), methane ($FE_M$), and ethylene ($FE_E$) in the temperature range of 293 to 323 K applied at constant current density = 45 mA·cm$^{-2}$, Bi *CL* = 0.75 mg·cm$^{-2}$, and relative humidity of 100%.

From the results obtained, the optimal operating condition for the electrocatalytic conversion of $CO_2$ to obtain formate using Bi/C-CCMEs is considered to be a temperature of 293 K. Similarly, when $CO_2$ electrovalorization to produce formate was carried out using Sn as the electrocatalyst in configuration CCMEs [52], this temperature was considered to be the optimal operating condition.

**Amount of water in the $CO_2$ stream**

Further experiments were carried out with the aim of analyzing the influence of the water flow in the input stream on the $CO_2$ electrocatalytic reduction to formate using this new

configuration of the G–L–S reaction system employing Bi/C-CCMEs as the working electrode. Before conducting these experiments, we hypothesized that the highest performance of this G–L–S system would be achieved when the amount of liquid in the system would be adequate for the progress of the reaction, but not so low as to hinder the reduction reaction or as high as to nullify the benefits arising from the use of a solid electrolyte. Under this operating condition, the performance higher than that of a conventional system with a liquid electrolyte could be achieved. Therefore, the analysis of the influence of the water input flow is essential for understanding reactor performance.

According to the results presented in the previous subsection on the influence of temperature, in these experiments, the temperature was fixed at 293 K. In addition, all the tests were performed using CCMEs with a *CL* of 0.75 mg·cm$^{-2}$ for carbon-supported Bi nanoparticles, and the current density supplied by a potentiostat-galvanostat was 45 mA·cm$^{-2}$. For each test, both phases were analyzed in order to determine the influence of the water flow in the $CO_2$ stream on $r_F$, *FE* of all products, *EC*, and *[HCOO$^-$]*. Figure 6 and 8 summarize the results obtained, while the detailed values are reported in Table S3 of the Supporting Information.

**Figure 6.** Influence of water flow in the $CO_2$ stream on (a) formate rate (mmol·m$^{-2}$·s$^{-1}$) and Faradaic efficiency for formate (%) and (b) the consumption of energy per kmol of formate (MJ·kmol$^{-1}$) and formate concentration (g·L$^{-1}$) in the water flow range of 0.15–1 g·h$^{-1}$ applied at constant current density = 45 mA·cm$^{-2}$, Bi *CL* = 0.75 mg·cm$^{-2}$, as measured at room temperature.

The lowest performance in terms of $r_F$ and $FE_F$ was observed when the $CO_2$ input stream introduced to the electrochemical reactor was not saturated (0.15 g·h$^{-1}$). These data points

correspond to a relative humidity of 66%. As illustrated in Figure 6a, increasing the water flow in the $CO_2$ stream from 0.15 to 0.227 $g \cdot h^{-1}$, which corresponds to the saturated conditions of the $CO_2$ stream introduced to the filter-press reactor, enhances the electrochemical process to give formate. On the one hand, $r_F$ and $FE_F$ increase by more than 19% with respect to the values of $r_F$ and $FE_F$ working with a non-saturated $CO_2$ stream, with values of 1.10 $mmol \cdot m^{-2} \cdot s^{-1}$ and 47.2%, respectively. In contrast, when the electrochemical reactor was fed with a saturated $CO_2$ stream, the *EC* decreased from 1224 to 1123.2 $MJ \cdot kmol^{-1}$, while $[HCOO^-]$ increased from 18.6 to 22.3 $g \cdot L^{-1}$, thus achieving an increase of approximately 8.2% and 20%, respectively (Figure 6b).

A possible explanation for these results may be related to the influence of the amount of water supplied to the liquid layer formed in the G–L–S reaction system, as schematically illustrated in Figure 7. The vapor supplied in the $CO_2$ stream introduced to the electrochemical reactor condenses over the CCME surface, forming a liquid film. In this way, the thickness of this liquid film depends on the amount of vapor condensed, and it also affects the ohmic resistance of the system. Therefore, the control of the water flow in the $CO_2$ stream is important in order to improve the performance of the G–L–S reaction system. These ideas are in accordance with Vennekoetter et al., who also points to the importance of controlling the thickness of the liquid layer and the hydrodynamics in the reactor for effective $CO_2$ conversion [47].

When the amount of water in the $CO_2$ input stream to the reactor was low (i.e., less than 0.5 $g \cdot h^{-1}$), the results suggest that the G–L–S reaction system was not operating under the optimal hydrodynamic conditions because the amount of water vapor condensed on the

CCME surface was not sufficient to form a liquid film of appropriate thickness (Figure 7a).

**Figure 7.** Schematic of liquid film formation over the CCME surface depending on the amount of water in the $CO_2$ stream: (a) scarce amount of water in the $CO_2$ input stream, (b) optimal amount of water in the $CO_2$ input stream (solid polymer electrolyte), and (c) excess amount of water in the $CO_2$ stream (liquid electrolyte).

Interestingly, as shown in Figure 6a, increasing the water flow in the $CO_2$ stream from 0.227 (which corresponds to a relative humidity of 100%) to 0.5 $g \cdot h^{-1}$ results in an important increase in $r_F$ and $FE_F$, from 1.10 $mmol \cdot m^{-2} \cdot s^{-1}$ and 47.2% to 1.28 $mmol \cdot m^{-2} \cdot s^{-1}$ and 54.8%, respectively. In contrast to the previous tests conducted at different water flow rates in the $CO_2$ stream, operating with 0.5 $g \cdot h^{-1}$ of water resulted in the optimal conditions for $CO_2$ electroconversion to formate using Bi/C-CCMEs. Consequently, under these operating conditions, it may be concluded that enough water is condensed on the electrode surface, resulting in the optimal hydrodynamic conditions in the G–L–S system for the $CO_2$ electroconversion process (Figure 7b).

However, a further increase in the water flow in the $CO_2$ stream to 1 $g \cdot h^{-1}$ lowered $r_F$ and $FE_F$. In terms of *EC* and $[HCOO^-]$, the optimum water flow in the $CO_2$ stream was also 0.5 $g \cdot h^{-1}$, achieving a value of 956.88 $MJ \cdot kmol^{-1}$ and 25.9 $g \cdot L^{-1}$, respectively (Figure 6). However, increasing the amount of water in the $CO_2$ stream from 0.5 to 1 $g \cdot h^{-1}$ decreased $[HCOO^-]$ from 25.9 to 22.6 $g \cdot L^{-1}$. At this water flow rate in the input $CO_2$ stream the electrochemical process was disturbed, increasing the liquid film over the CCMEs and inhibiting the input of the $CO_2$ stream to the catalytic layer of the working electrode. In

this way, the thickness of the liquid film provides a larger distance between the catalytic surface of the working electrode and the surface of the liquid film formed (Figure 7c). Therefore, the electrochemical cell potential increased (see values in Table S3 of the Supporting Information) as water flow in the $CO_2$ stream increased. Moreover, this excess water flow in the $CO_2$ stream also affected the behavior of the filter-press reactor, approximating the performance of a conventional system in which the catholyte acts as a liquid electrolyte and dilutes the reaction products in the output stream of the reactor.

In addition to reporting liquid phase analysis, the gas phase was also analyzed in order to gain additional understanding of the $CO_2$ electrochemical process. Figure 8 summarizes the influence of water flow in the $CO_2$ stream on the *FE* of the products detected in both phases (values are described in Table S4 of the Supporting Information). It should be noted that the same gaseous products as in the experiments reported in the previous subsection at different temperatures (Figure 5) are detected ($H_2$, CO, $CH_4$, and $C_2H_4$).

**Figure 8.** Influence of water input flow in the $CO_2$ stream on *FE* to formate ($FE_F$), hydrogen ($FE_H$), carbon monoxide ($FE_C$), methane ($FE_M$), and ethylene ($FE_E$) in the water flow range of 0.15–1 $g \cdot h^{-1}$ applied at constant current density = 45 $mA \cdot cm^{-2}$, Bi *CL* = 0.75 $mg \cdot cm^{-2}$, as measured at room temperature.

Working with a $CO_2$ stream non-saturated with $H_2O$ (which corresponds to a water flow in the $CO_2$ stream of 0.15 $g \cdot h^{-1}$), the main product detected was $H_2$, with an $FE_H$ of 46.1%, with formate detected with an $FE_F$ of 39.4%. Note that, as depicted in Figure 8, when the $CO_2$ electroreduction process to formate proceeds with a water flow of 0.15 $g \cdot h^{-1}$ or a non-saturated stream of $CO_2$, formate is not the main product detected in both phases. As shown in Figure 6a, increasing the water flow in the $CO_2$ stream to 0.5 $g \cdot h^{-1}$, the optimal

performance of the electrochemical process is achieved, yielding an $FE_F$ of 54.8%. Operating under these conditions, an $FE_H$ of 40.9% is obtained, approximately 12.5% lower than that when operating with a water flow of 0.15 $g \cdot h^{-1}$. However, increasing the water flow from 0.52 $g \cdot h^{-1}$ (see values in Table S4 of the Supporting Information), $FE_F$ decreased to 41.1% (approximately 25% lower). Thus, this decrease in $FE_F$ leads to an increase in $FE_H$, from 40.9% to 46.1% (corresponding to a water flow of 2 $g \cdot h^{-1}$), which may be attributed to the fact that the excess water condensed over the surface could improve the hydrogen evolution reaction. As seen in Figure 8, $FE_C$ and $FE_M$ are similar for the range of the water flow studied, approximately 10% and 2%, respectively. In addition, $C_2H_4$ was detected using a non-saturated $CO_2$ stream (0.15 $g \cdot h^{-1}$ of water flow) or with a $CO_2$ stream with a flow of 2 $g \cdot h^{-1}$. It should be noted that the accumulated *FE* for these products detected in both phases was approximately 100% in all tests.

**Further improvements in G–L–S reaction system performance**

Additional tests were carried out in an attempt to improve the performance of the G–L–S system for the electrochemical conversion of $CO_2$ to formate using Bi/C-CCMEs. According to the results reported in the previous section, these tests were conducted at room temperature (293 K) to achieve the highest performance of the reaction system. These additional experiments focus on further analyzing the influence of i) increasing the *CL* in the CCME, and ii) increasing the current density (*J*) at which the process is performed.

**Increasing the catalyst loading *CL***

First, the *CL*, is increased to 1.5 mg·cm$^{-2}$, instead of 0.75 mg·cm$^{-2}$. As in previous section, these experiments were conducted to investigate the influence of the vapor supplied in the $CO_2$ stream and introduced to the electrochemical reactor, analyzing both the liquid and gas phases, and operating with a constant $J$ = 45 mA·cm$^{-2}$.

The effects of vapor supplied in the $CO_2$ stream on $FE_F$ (Figure 9a), *[HCOO$^-$]* (Figure 9b), $r_F$ (Figure S2a), and *EC* (Figure S2b) and the comparison with electrodes with a *CL* of 0.75 mg·cm$^{-2}$ were studied (values are described in Table S5 in the Supporting Information). The range of water flow in the analyzed $CO_2$ stream is between 0.5 g·h$^{-1}$ (which corresponds to the optimal behavior at *CL* of 0.75 mg·cm$^{-2}$) and 5 g·h$^{-1}$. Although at a water flow in the $CO_2$ stream of 0.5 g·h$^{-1}$ the resulting $r_F$ and $FE_F$ are similar for both *CL*s of 1.3 mmol·m$^{-2}$·s$^{-1}$ and 55%, respectively, the highest performance of the working electrode with a *CL* of 1.5 mg·cm$^{-2}$ is achieved when the amount of vapor supplied in the $CO_2$ stream increases. The highest performance is obtained with a flow of vapor in a $CO_2$ stream of 3 g·h$^{-1}$, instead of introducing 0.5 g·h$^{-1}$ with a *CL* of 0.75 mg·cm$^{-2}$. However, increasing the water flow in the $CO_2$ stream from 3 to 5 g·h$^{-1}$, both $r_F$ and $FE_F$ decrease to 1.31 mmol·m$^{-2}$·s$^{-1}$ and 56%, respectively, 21% lower than those under the optimal conditions.

**Figure 9.** Influence of water flow in the $CO_2$ stream on (a) Faradaic efficiency for formate (%) and (b) formate concentration (g·L$^{-1}$) working with Bi/C-CCMEs with a Bi *CL* = 0.75 mg·cm$^{-2}$ and 1.5 mg·cm$^{-2}$ in the water flow range of 0.5–5 g·h$^{-1}$ at a constant current density of 45 mA·cm$^{-2}$ as measured at room temperature.

In terms of *[HCOO$^-$]* (Figure 9b) and *EC* (Figure S2b), the performance of the electrochemical reactor is similar to that discussed in Figure 9. On the one hand, the optimal result was obtained when the filter-press cell is fed with a water flow of 3 g·h$^{-1}$. In contrast, increasing the vapor supplied in the $CO_2$ stream yields unsatisfactory results for *[HCOO$^-$]* and *EC*, decreasing *[HCOO$^-$]* from 34 to 27 g·L$^{-1}$ and increasing *EC* from 835.2 to 1080 MJ·kmol$^{-1}$.

Therefore, using a working electrode with a *CL* of 1.5 g·cm$^{-2}$ leads to higher performance than that at a *CL* of 0.75 mg·cm$^{-2}$, considering the criteria analyzed: $r_F$, $FE_F$, *[HCOO$^-$]*, and *EC*. The performance of the electrochemical process was similar under both conditions. Similarly, the amount of water that condenses over the CCME surface must be optimized in order to achieve optimal hydrodynamic conditions in the electrochemical reactor. Increasing the *CL* of Bi deposited over the electrode from 7.5 to 15 mg resulted in the optimal conditions, under which the water flow rate introduced in the $CO_2$ stream could be increased from 0.5 to 3 g·h$^{-1}$. As discussed in the previous section, the water condensing over the electrode is responsible for the thickness of the liquid film over the electrode surface, this thickness directly affects the ohmic resistance of the electrochemical reactor. Thus, when operating at a water flow in the $CO_2$ input stream of 3 g·h$^{-1}$, it may be argued that the distance between the liquid film and the catalyst affects the input of $CO_2$ to the electrode surface. However, when the water flow increases to 5 g·h$^{-1}$, the thickness of the liquid film increases, resulting in poor hydrodynamic conditions and interaction between the G–L–S phases, $CO_2$, and electrode surface.

Apart from the production of formate in the liquid phase, other products were detected in the gas phase, such as $H_2$, CO, and $CH_4$, when working with a *CL* of 1.5 mg·cm$^{-2}$. As illustrated in Figure 10 (values are reported in Table S6 of the Supporting Information), the influence of the vapor supplied to the electrochemical reactor was studied in terms of $FE_F$, $FE_H$, $FE_C$, and $FE_M$. As explained previously, $FE_F$ has its optimal value operating at a water flow of 3 g·h$^{-1}$ under the operating condition of $FE_H$ of 22.3%, $FE_C$ of 7.5%, and $FE_M$ of 3.7%. At 0.5–5 g·h$^{-1}$, the $FE_C$ and $FE_M$ values were similar. However, $FE_H$ has an important fluctuation operating at different water flows in the $CO_2$ stream fed to the electrochemical filter-press. Increasing the water flow from the optimal value to 5 g·h$^{-1}$ results in an increase in $FE_H$, increasing approximately 54% than when operating at 3 g·h$^{-1}$. As explained in the last section (*CL* of 0.75 mg·cm$^{-2}$), increasing the water flow favors the hydrogen evolution reaction, which explains the higher production of hydrogen observed. Furthermore, it is important to consider that the *FE* accumulated for all the products detected in both the liquid and gas phases ranged between 98% and 105%.

**Figure 10.** Influence of water input flow in the $CO_2$ stream on FE to formate ($FE_F$), hydrogen ($FE_H$), carbon monoxide ($FE_C$), and methane ($FE_M$) working with Bi/C-CCMEs with a Bi *CL* = 1.5 mg·cm$^{-2}$ in the water flow range of 0.5–5 g·h$^{-1}$ applied at a constant current density of 45 mA·cm$^{-2}$, as measured at room temperature.

**Increasing the current density *J***

According to previous results, additional experiments were carried out in order to study the influence of *J* on $CO_2$ electroconversion to formate using working electrodes with different *CL* operating under the optimal conditions of water flow in the $CO_2$ stream. As

discussed in the previous subsection, the electroreduction of $CO_2$ to formate at a *CL* of 1.5 mg·cm$^{-2}$ gives better results than that at a *CL* of 0.75 mg·cm$^{-2}$. For this reason, the figures showing the influence of *J* on $r_F$, $FE_F$, *[HCOO$^-$]*, and *EC* with *J* at *CL* of 0.75 mg·cm$^{-2}$ are included in the Supporting Information (Figure S3). In addition, the values are reported in Table S7 of the Supporting Information.

The electrochemical conversion of $CO_2$ was studied for a *CL* of 1.5 mg·cm$^{-2}$ with an optimal water flow of 3 g·h$^{-1}$, as studied in the previous subsection. Figure 11a shows the influence of *J* on $r_F$ and $FE_F$, whereas Figure 11b also displays the effect of *J* on *EC* and *[HCOO$^-$]* (values are described in Table S8 in the Supporting Information). When increasing *CL*, the behavior of the electrochemical reactor is similar to when *J* is increased. An $r_F$ of 3.06 mmol·m$^{-2}$·s$^{-1}$ and a noteworthy *[HCOO$^-$]* of 46.5 g·L$^{-1}$ is obtained when *J* increases from 45 to 200 mA·cm$^{-2}$. Nevertheless, $FE_F$ and *EC* decrease when *J* is increased, achieving values of 46.1% and 1452.24 MJ·kmol$^{-1}$, respectively.

**Figure 11.** Influence of current density on (a) formate rate (mmol·m$^{-2}$·s$^{-1}$) and Faradaic efficiency for formate (%) and (b) consumption of energy per kmol of formate (MJ·kmol$^{-1}$) and formate concentration (g·L$^{-1}$) in the current density range of 45–200 mA·cm$^{-2}$ operating at 293 K, Bi *CL* = 1.5 mg·cm$^{-2}$, and water flow in the $CO_2$ stream = 3 g·h$^{-1}$.

## Conclusions

In this study, continuous $CO_2$ electroreduction to formate in a G–L–S reaction system was developed with a single pass of the $CO_2$ humidified stream through the electrochemical reactor. The cathodes were prepared by airbrushing the Bi/C NPs directly over the Nafion 117 membrane. Both the liquid and gas phases were analyzed. In the

liquid phase, only formate was detected in all experiments with traces of alcohols. The influence of temperature and the amount of water in the $CO_2$ input stream were studied. The results show that it is possible to improve the performance of a G–L–S reaction system operating at room temperature by varying the water content of the input stream, instead of operating with a saturated stream and increasing the water content by increasing the temperature of the input stream, resulting in a system with the advantage of operating at room temperature. Concentrations of $HCOO^-$ of up to 25.9 $g \cdot L^{-1}$ were achieved operating at a temperature of 293 K and with a water flow in the $CO_2$ stream of 0.5 $g \cdot h^{-1}$. This could be attributed to the fact that under these operating conditions the thickness of the liquid film that coats the Bi/C-CCME surface is optimal for performance. Increasing the water flow in the $CO_2$ input stream hinders the performance of the electrochemical reactor, with performance approaching that of a corresponding liquid electrolyte reactor. This is because of the hydrodynamic conditions, which lead to an increase in the ohmic resistance of the electrochemical reactor. For this reason, when the water flow in the $CO_2$ stream was increased, the performance of the electrochemical conversion of $CO_2$ to formate decreased in terms of the $r_F$, $FE_F$, $[HCOO^-]$, and *EC*. More work is in progress to properly understand the fundamental aspects involved in these findings in terms of $CO_2$ reaction mechanisms, pathways, and intermediates. This fundamental understanding will help to fully explain the experimental results reported in this paper, and also to improve them.

Further experiments were developed with the aim of improving the performance of the G–L–S reaction system. When the Bi *CL* was increased from 0.75 $mg \cdot cm^{-2}$ to 1.5 $mg \cdot cm^{-}$

$^{2}$, a larger amount of water in the $CO_2$ input stream was required (3 $g \cdot h^{-1}$) in order to achieve the optimal hydrodynamic conditions for the electrochemical reactor. The optimal result was obtained when the electrochemical reactor was fed with a water flow in the $CO_2$ stream of 3 $g \cdot h^{-1}$, achieving a $[HCOO^-]$ and $FE_F$ value of 34 $g \cdot L^{-1}$ and 72%, respectively. Moreover, $[HCOO^-]$ could be increased (46.5 $g \cdot L^{-1}$) when $J$ was increased from 45 $mA \cdot cm^{-2}$ to 200 $mA \cdot cm^{-2}$, but at the expense of a decrease in $FE_F$. It is important to note that the results of this study have been obtained in a continuous G–L–S reaction system, working with a single pass of the $CO_2$ humidified stream through the electrochemical reactor. However, further research is still required to improve the performance of the G–L–S reaction system for the electrocatalytic conversion of $CO_2$ to formate using Bi/C-CCMEs for the future implementation of the electrochemical process at the industrial scale.

**Acknowledgments**

The authors of this work would like to acknowledge the financial support from the MINECO through the projects CTQ2016-76231-C2-1-R and CTQ2016-76231-C2-2-R (AEI/FEDER, UE). JSG acknowledges financial support from VITC (Vicerrectorado de Investigación y Transferencia de Conocimiento) of the University of Alicante (UTALENTO16-02).

**References**

1. Paris Agreement Climate Action, European Commission.

https://ec.europa.eu/clima/policies/international/negotiations/paris_en (accessed November 01, 2019).

2. Overview of Greenhouse Gases, United States Environmental Protection Agency. https://www.epa.gov/ghgemissions/overview-greenhouse-gases (accessed November 01, 2019).

3. Zhang W, Hu Y, Ma L, Zhu G, Wang Y, Xue X, Chen R, Yang S, Jin Z. Progress and Perspective of Electrocatalytic $CO_2$ Reduction for Renewable Carbonaceous Fuels and Chemicals. *Adv Sci*. 2018;5(1):1700275.

4. Bevilacqua M, Filippi J, Miller HA, Vizza F. Recent technological progress in $CO_2$ electroreduction to fuels and energy carriers in aqueous environments. *Energy Technol*. 2015;3(3):197-210.

5. Qiao J, Liu Y, Zhan J. Electrochemical Reduction of Carbon Dioxide. Fundamentals and Technologies. CRC Press, Boca Raton, 2016.

6. Baena-Moreno FM, Rodríguez-Galán M, Vega F, Alonso-Fariñas B, Vilches Arenas LF, Navarrete B. Carbon capture and utilization technologies: a literature review and recent advances. *Energy Sources, Part A Recover Util Environ Eff*. 2019;41(12):1403-1433.

7. Irabien A, Alvarez-Guerra M, Albo J, Domínguez-Ramos A. Electrochemical conversion of $CO_2$ to value-added products. In: Martínez-Huitle CA, Rodrigo MA, Scialdone O. Electrochememical Water Wastewater Treatment. Elsevier,2018:29-59.

8. Hori Y. Reduction using Electrochemical approach. In: Sugiyama M, Fujii K, Nakamura S. Solar to Chemical Energy Conversion: Theory and Application. Cham 2016:191-211.

9. Olajire AA. Recent progress on the nanoparticles-assisted greenhouse carbon dioxide conversion processes. *J $CO_2$ Util*. 2018;24:522-547.

10. Zheng Y, Zhang W, Li Y, Chen J, Yu B, Wang J, Zhang L, Zhang J. Energy related $CO_2$ conversion and utilization: Advanced materials/nanomaterials, reaction mechanisms and technologies. *Nano Energy*. 2017;40:512-539.

11. Castro S, Albo J, Irabien A. Photoelectrochemical Reactors for $CO_2$ Utilization. *ACS Sustain Chem Eng*. 2018;6(12):15877-15894.

12. Kumar B, Brian JP, Atla V, Kumari S, Bertram KA, White RT, Spurgeon JM. New trends in the development of heterogeneous catalysts for electrochemical $CO_2$ reduction. *Catal Today*. 2016;270:19-30.

13. Martín AJ, Larrazábal GO, Pérez-Ramírez J. Towards sustainable fuels and chemicals through the electrochemical reduction of $CO_2$: lessons from water electrolysis. *Green Chem*. 2015;17(12):5114-5130.

14. Lu Q, Jiao F. Electrochemical $CO_2$ reduction: Electrocatalyst, reaction mechanism, and process engineering. *Nano Energy*. 2016;29:439-456.

15. Masel R, Liu Z, Zhao D, Chen Q, Lutz D, Nereng L. $CO_2$ Conversion to Chemical with Emphasis on using Renewable Energy/Resources to Drive the conversion. In:

Clark J, Kraus GA, Stankiewiez A, Siedl P. Commercializing Biobased Products: Opportunities, Challenges, Benefits and Risk. RSC Green Chemistry, 2016:215–257.

16. Merino-Garcia I, Alvarez-Guerra E, Albo J, Irabien A. Electrochemical membrane reactors for the utilisation of carbon dioxide. *Chem Eng J*. 2016;305:104-120.

17. Du D, Lan R, Humphreys J, Tao S. Progress in inorganic cathode catalysts for electrochemical conversion of carbon dioxide into formate or formic acid. *J Appl Electrochem*. 2017;47:661-678.

18. Nielsen DU, Hu XM, Daasbjerg K, Skrydstrup T. Chemically and electrochemically catalysed conversion of $CO_2$ to CO with follow-up utilization to value-added chemicals. *Nat Catal*. 2018;1(4):244-254.

19. Gao D, Arán-Ais RM, Jeon HS, Roldan Cuenya B. Rational catalyst and electrolyte design for $CO_2$ electroreduction towards multicarbon products. *Nat Catal*. 2019;2:198-210.

20. An L, Chen R. Direct formate fuel cells: A review. *J Power Sources*. 2016;320:127-139.

21. Preuster P, Albert J. Biogenic Formic Acid as a Green Hydrogen Carrier. *Energy Technol*. 2018;6(3):501-509.

22. Liu G, Li Z, Shi J, Sun K, Ji Y, Wang Z, Qiu Y, Liu Y, Wang Z, Hu P. Black reduced porous $SnO_2$ nanosheets for $CO_2$ electroreduction with high formate

selectivity and low overpotential. *Appl Catal B Environ*. 2020;260:118134.

23. Lee W, Kim YE, Youn MH, Jeong SK, Park KT. Catholyte-Free Electrocatalytic $CO_2$ Reduction into Formate.*Angew Chemie Int Ed*. 2018;57:6883-6887.

24. Proietto F, Schiavo B, Galia A, Scialdone O. Electrochemical conversion of $CO_2$ to HCOOH at tin cathode in a pressurized undivided filter-press cell. *Electrochim Acta*. 2018;277:30-40.

25. Yang H, Kaczur JJ, Sajjad SD, Masel RI. Electrochemical conversion of $CO_2$ to formic acid utilizing Sustainion™ membranes. *J $CO_2$ Util*. 2017;20:208-217.

26. Yang H, Kaczur JJ, Sajjad SD, Masel RI. $CO_2$ Conversion to Formic Acid in a Three Compartment Cell with Sustainion™ Membranes. *ECS Trans*. 2017;77(11):1425-1431.

27. Scialdone O, Galia A, Nero G Lo, Proietto F, Sabatino S, Schiavo B. Electrochemical reduction of carbon dioxide to formic acid at a tin cathode in divided and undivided cells: Effect of carbon dioxide pressure and other operating parameters. *Electrochim Acta*. 2016;199:332-341.

28. An X, Li S, Yoshida A, Wang Z, Hao X, Abudula A, Guan G. Electrodeposition of Tin-Based Electrocatalysts with Different Surface Tin Species Distributions for Electrochemical Reduction of $CO_2$ to HCOOH. *ACS Sustain Chem Eng*. 2019;7(10):9360-9368.

29. Choi SY, Jeong SK, Kim HJ, Baek IH, Park KT. Electrochemical Reduction of

Carbon Dioxide to Formate on Tin-Lead Alloys. *ACS Sustain Chem Eng*. 2016;4(3):1311-1318.

30. Pander JE, Lum JWJ, Yeo BS. The importance of morphology on the activity of lead cathodes for the reduction of carbon dioxide to formate. *J Mater Chem A*. 2019;7(8):4093-4101.

31. Lee CH, Kanan MW. Controlling $H^+$ vs $CO_2$ Reduction Selectivity on Pb Electrodes. *ACS Catal*. 2015;5(1):465-469.

32. Alvarez-Guerra M, Quintanilla S, Irabien A. Conversion of carbon dioxide into formate using a continuous electrochemical reduction process in a lead cathode. *Chem Eng J*. 2012;207-208:278-284.

33. Mou K, Chen Z, Yao S, Liu, L. Enhanced electrochemical reduction of carbon dioxide to formate with in-situ grown indium-based catalysts in an aqueous electrolyte. *Electrochim. Acta* 2018;289:65-71.

34. Luo W, Xie W, Li M, Zhang J, Züttel A. 3D hierarchical porous indium catalyst for highly efficient electroreduction of $CO_2$. *J Mater Chem A*. 2019;7(9):4505-4515.

35. Klinkova A, De Luna P, Dinh CT, Voznyy O, Larin EM, Kumacheva E, Sargent EH. Rational Design of Efficient Palladium Catalysts for Electroreduction of Carbon Dioxide to Formate. *ACS Catal*. 2016;6(12):8115-8120.

36. Bai X, Chen W, Zhao C, Li S, Song Y, Ge R, Wei W, Sun Y. Exclusive Formation

of Formic Acid from $CO_2$ Electroreduction by a Tunable Pd-Sn Alloy. *Angew Chemie - Int Ed*. 2017;56(40):12219-12223.

37. Han N, Wang Y, Yang H, Deng J, Wu J, Li Y, Li Y. Ultrathin bismuth nanosheets from in situ topotactic transformation for selective electrocatalytic $CO_2$ reduction to formate. *Nat Commun*. 2018;9(1):1-8.

38. Atifi A, Boyce DW, Dimeglio JL, Rosenthal J. Directing the Outcome of $CO_2$ Reduction at Bismuth Cathodes Using Varied Ionic Liquid Promoters. *ACS Catal*. 2018;8(4):2857-2863.

39. Qiu Y, Du J, Dong W, Dai C, Tao C. Selective conversion of $CO_2$ to formate on a size tunable nano-Bi electrocatalyst. *J $CO_2$ Util*. 2017;20:328-335.

40. Wen G, Lee DU, Ren B, Hassan FM, Jiang G, Cano ZP, Gostick J, Croiset E, Bai Z, Yang L, Chen Z. Orbital Interactions in Bi-Sn Bimetallic Electrocatalysts for Highly Selective Electrochemical $CO_2$ Reduction toward Formate Production. *Adv Energy Mater*. 2018;8(31):1-9.

41. Xia C, Zhu P, Jiang Q, Pan Y, Liang W, Stavitsk E. Continuous production of pure liquid fuel solutions via electrocatalytic $CO_2$ reduction using solid-electrolyte devices. *Nat. Energy* 2019;4:776-785.

42. Tran-Phu T, Daiyan R, Fusco Z, Ma Z, Amal R, Tricoli A. Nanostructured β-$Bi_2O_3$ Fractals on Carbon Fibers for Highly Selective $CO_2$ Electroreduction to Formate. *Adv Funct Mater*. 2019;30:1906478.

43. Yang F, Elnabawy AO, Schimmenti R, Song P, Wang J, Peng Z, Yao S, Deng R, Song S, Lin Y, Mavrikakis M, Xu W. Bismuthene for highly efficient carbon dioxide electroreduction reaction. *Nat Commun*. 2020;11(1):1088.

44. Kim S, Dong WJ, Gim S, Sohn W, Park JY, Yoo CJ, Jang HW, Lee J. Shape-controlled bismuth nanoflakes as highly selective catalysts for electrochemical carbon dioxide reduction to formate. *Nano Energy*. 2017;39:44-52.

45. Lv W, Bei J, Zhang R, Wang W, Kong F, Wang L, Wang W. $Bi_2O_2CO_3$ Nanosheets as Electrocatalysts for Selective Reduction of $CO_2$ to Formate at Low Overpotential. *ACS Omega*. 2017;2(6):2561-2567.

46. Zhang X, Lei T, Liu Y, Qiao J. Enhancing $CO_2$ electrolysis to formate on facilely synthesized Bi catalysts at low overpotential. *Appl Catal B Environ*. 2017;218:46-50.

47. Vennekoetter JB, Sengpiel R, Wessling M. Beyond the catalyst: How electrode and reactor design determine the product spectrum during electrochemical $CO_2$ reduction. *Chem Eng J*. 2019;364:89-101.

48. Alvarez-Guerra M, Del Castillo A, Irabien A. Continuous electrochemical reduction of carbon dioxide into formate using a tin cathode: Comparison with lead cathode. *Chem Eng Res Des*. 2014;92:692-701.

49. Castillo A Del, Alvarez-Guerra M, Solla-Gullón J, Sáez A, Montiel V, Irabien A. Sn nanoparticles on gas diffusion electrodes: Synthesis, characterization and use for continuous $CO_2$ electroreduction to formate. *J $CO_2$ Util*. 2017;18:222-228.

50. Del Castillo A, Alvarez-Guerra M, Irabien A. Continuous electroreduction of $CO_2$ to formate using Sn gas diffusion electrodes. *AIChE J*. 2014;60:3557-3564.

51. Díaz-Sainz G, Alvarez-Guerra M, Solla-Gullón J, García-Cruz L, Montiel V, Irabien A. $CO_2$ electroreduction to formate: Continuous single-pass operation in a filter-press reactor at high current densities using Bi gas diffusion electrodes. *J $CO_2$ Util*. 2019;34:12-19.

52. Díaz-Sainz G, Alvarez-Guerra M, Solla-Gullón J, García-Cruz L, Montiel V, Irabien A. Catalyst coated membrane electrodes for the gas phase $CO_2$ electroreduction to formate. *Catal Today*. 2020;346:58-64.

53. Ávila-Bolívar B, García-Cruz L, Montiel V, Solla-Gullón J. Electrochemical Reduction of $CO_2$ to Formate on Easily Prepared Carbon-Supported Bi Nanoparticles. *Molecules*. 2019;24(11):2032.

54. Kim HY, Choi I, Ahn SH, Hwang SJ, Yoo SJ, Han Y, Kim J, Park H, Jang JH, Kim S. Analysis on the effect of operating conditions on electrochemical conversion of carbon dioxide to formic acid. *Int J Hydrogen Energy*. 2014;39(29):16506-16512.

55. Zhang L, Zhao ZJ, Gong J. Nanostructured Materials for Heterogeneous Electrocatalytic $CO_2$ Reduction and their Related Reaction Mechanisms. *Angew Chemie - Int Ed.* 2017;56(38):11326-11353.

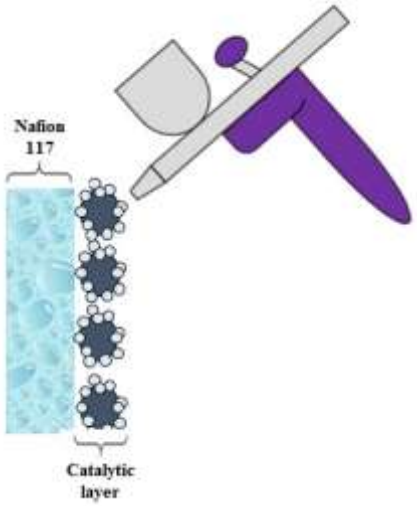


**Fig. 1.** Schematic of the airbrushing technique used to fabricate Bi/C-CCMEs.

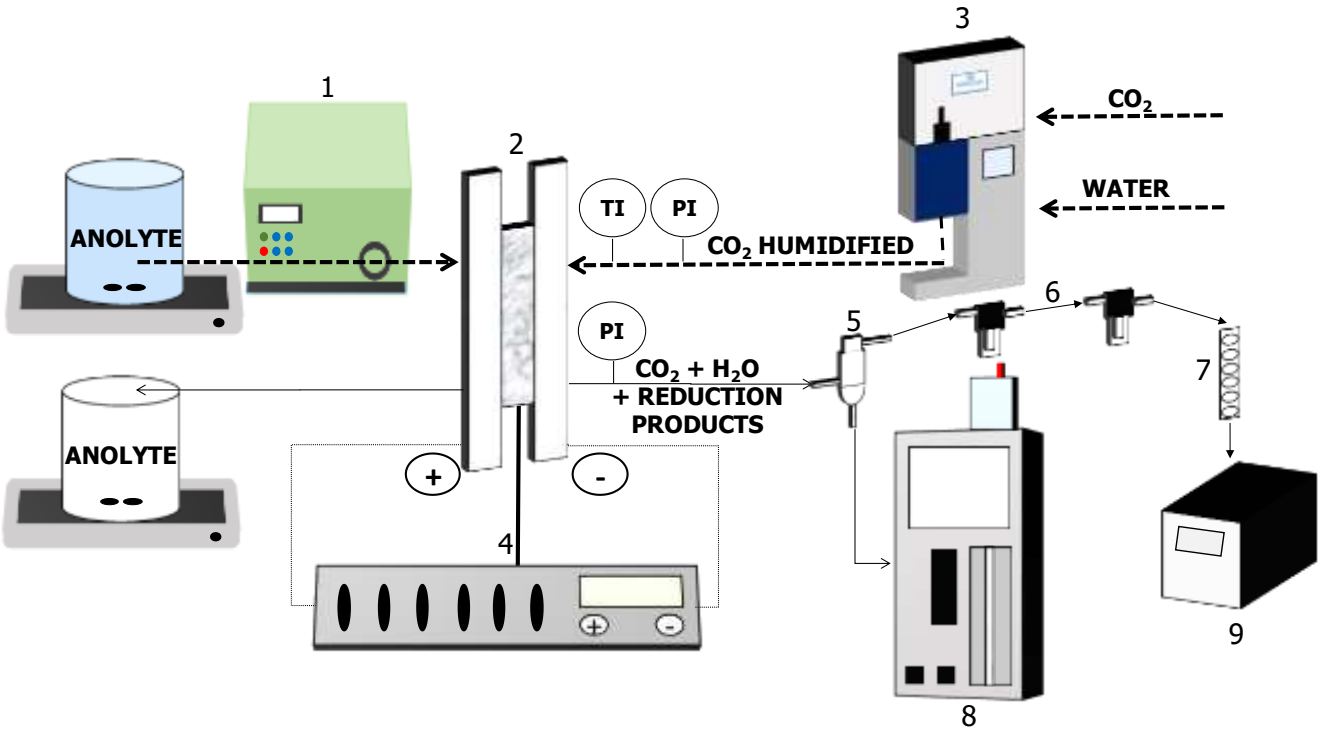


**Fig. 2.** Experimental setup used for the tests of Bi/C-CCMEs for the study of $CO_2$ electrochemical reduction to obtain $HCOO^-$: 1 (Peristaltic pump); 2 (Filter press reactor); 3 (Vapor Delivery Module); 4 (Potentiostat-galvanostat); 5 (G/L Separator); 6 (Filters); 7 (Trap); 8 (Ion chromatography); 9 (Gas chromatography).

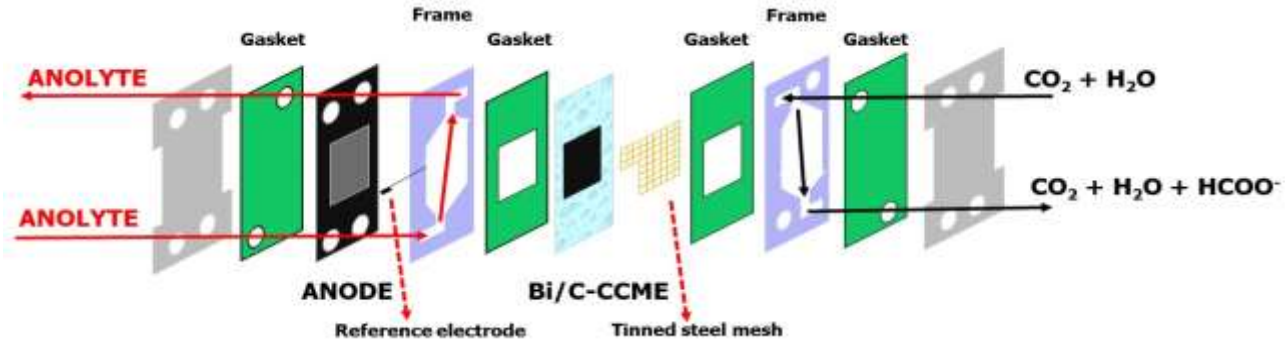


**Fig. 3.** Electrochemical filter-press reactor configuration for the tests of Bi/C-CCMEs used for the continuous electroreduction of $CO_2$ to obtain $HCOO^-$.

.

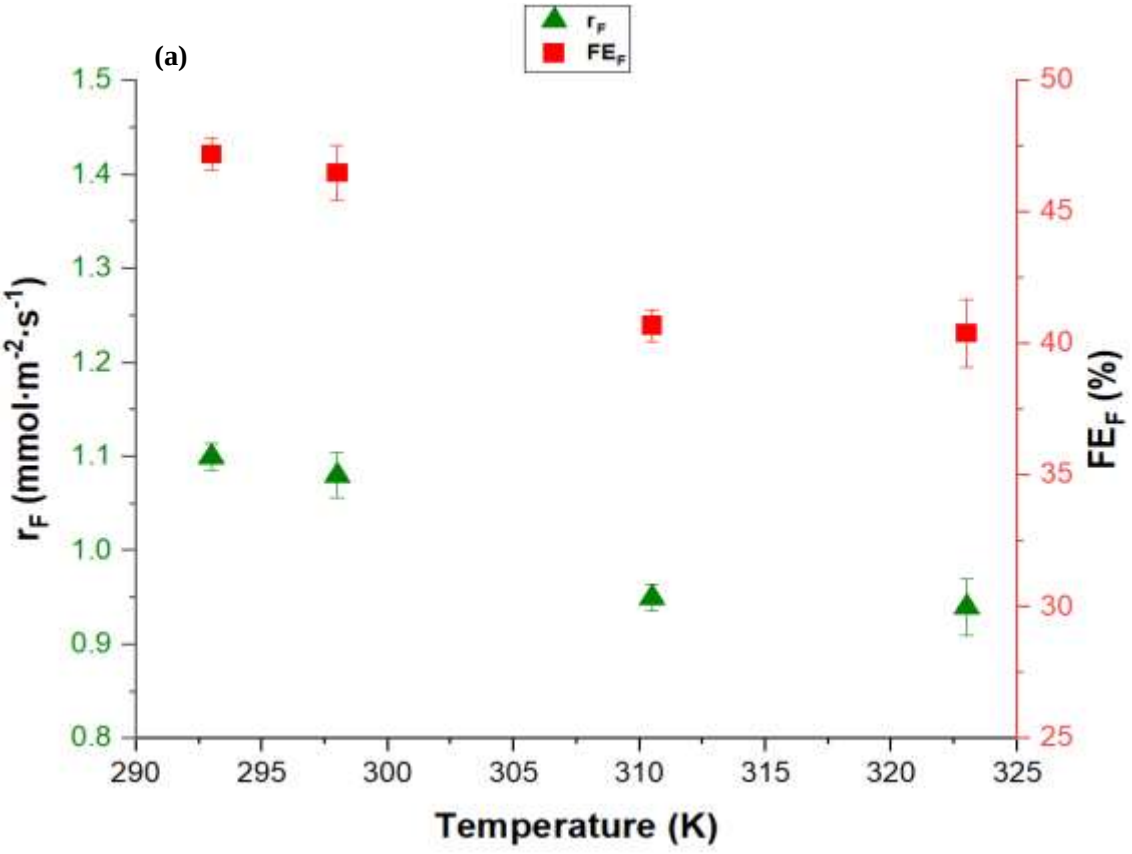


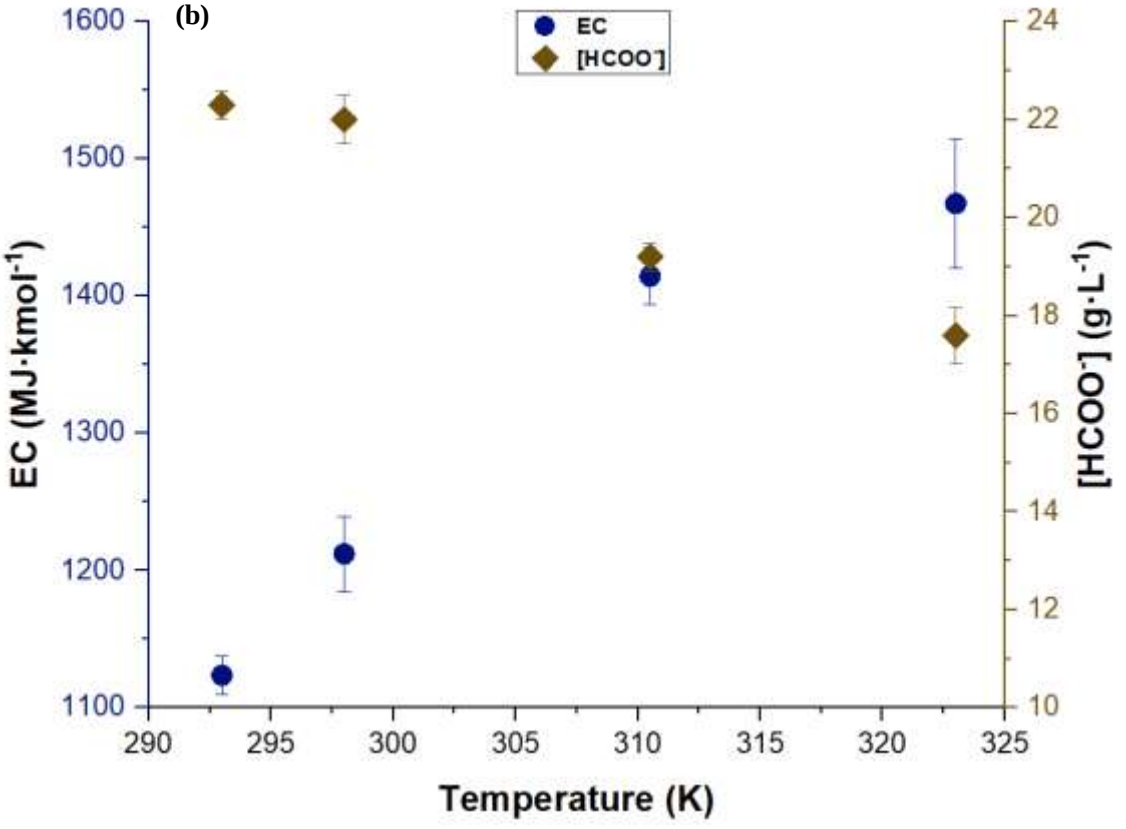

**Fig. 4.** Influence of temperature on (a) formate rate ($mmol \cdot m^{-2} \cdot s^{-1}$) and Faradaic efficiency for formate (%) and (b) the consumption of energy per kmol of formate ($MJ \cdot kmol^{-1}$) and Formate concentration ($g \cdot L^{-1}$) in the temperature range of 293–323 K applied at constant current density = 45 $mA \cdot cm^{-2}$, Bi CL = 0.75 $mg \cdot cm^{-2}$, and relative humidity = 100%.

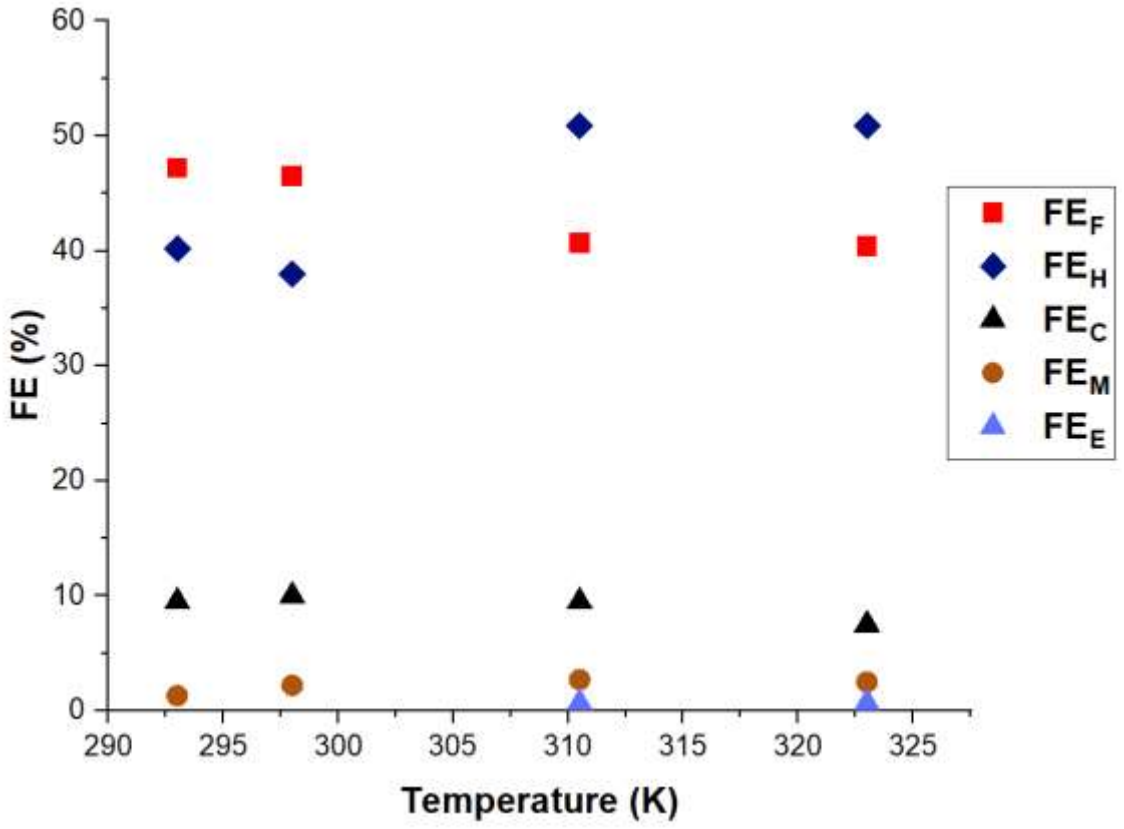


**Fig. 5.** Influence of temperature on the *FE* of formate ($FE_F$), hydrogen ($FE_H$), carbon monoxide ($FE_C$), methane ($FE_M$), and ethylene ($FE_E$) in the temperature range of 293 to 323 K applied at constant current density = 45 mA·cm$^{-2}$, Bi *CL* = 0.75 mg·cm$^{-2}$, and relative humidity of 100%.

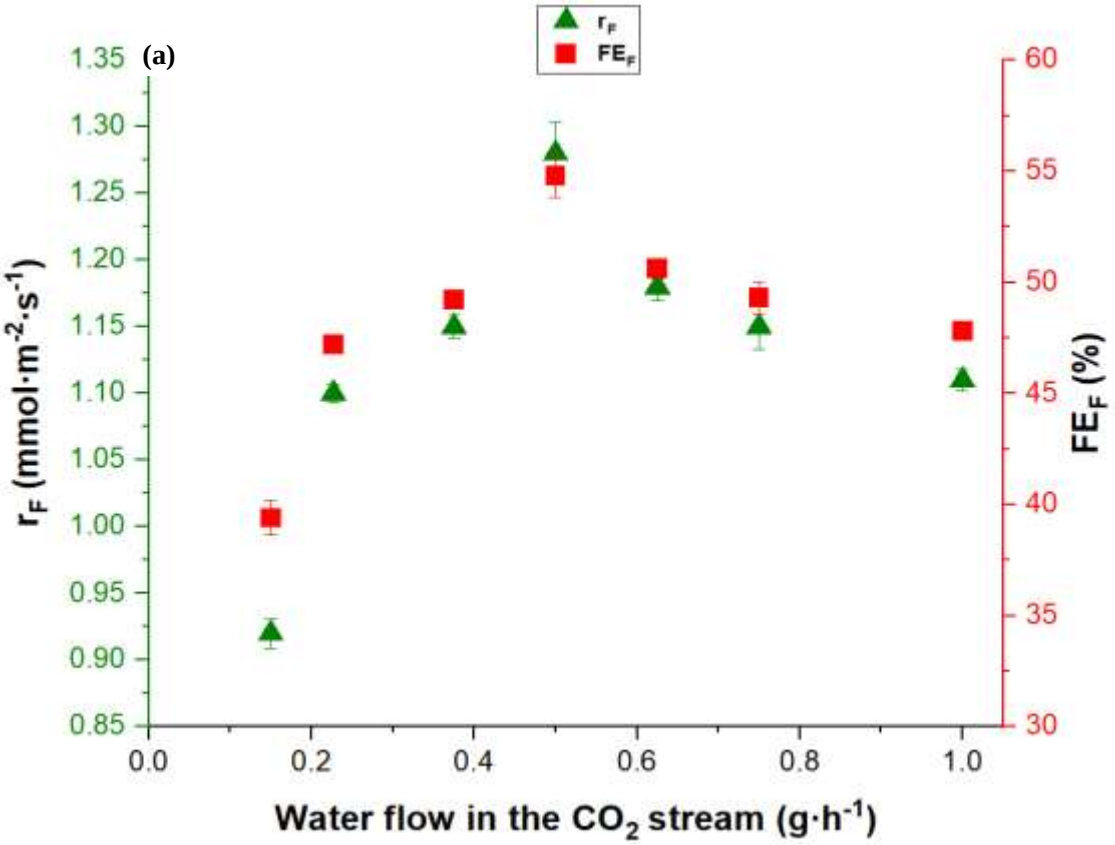


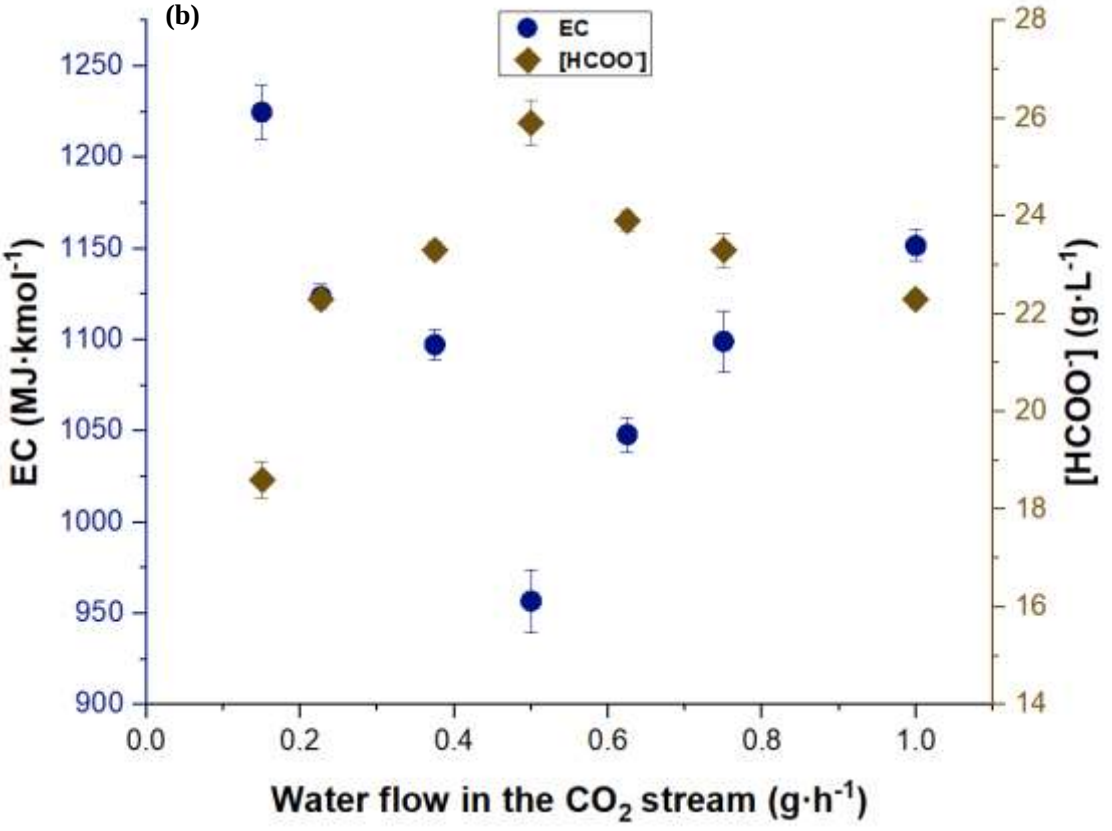

**Fig. 6.** Influence of water flow in the $CO_2$ stream on (a) formate rate ($mmol \cdot m^{-2} \cdot s^{-1}$) and Faradaic efficiency for formate (%) and (b) the consumption of energy per kmol of formate ($MJ \cdot kmol^{-1}$) and formate concentration ($g \cdot L^{-1}$) in the water flow range of 0.15–1 $g \cdot h^{-1}$ applied at constant current density = 45 $mA \cdot cm^{-2}$, Bi *CL* = 0.75 $mg \cdot cm^{-2}$, as measured at room temperature.

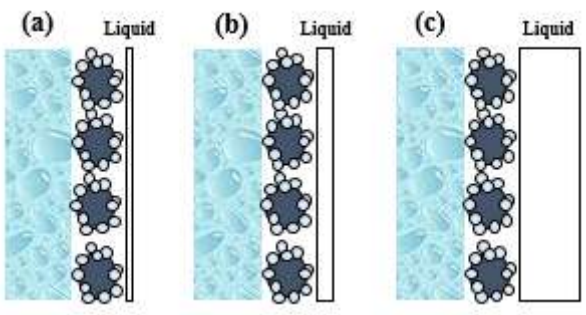

**Fig. 7.** Schematic of liquid film formation over the CCME surface depending on the amount of water in the $CO_2$ stream: (a) scarce amount of water in the $CO_2$ input stream, (b) optimal amount of water in the $CO_2$ input stream (solid polymer electrolyte), and (c) excess amount of water in the $CO_2$ stream (liquid electrolyte).

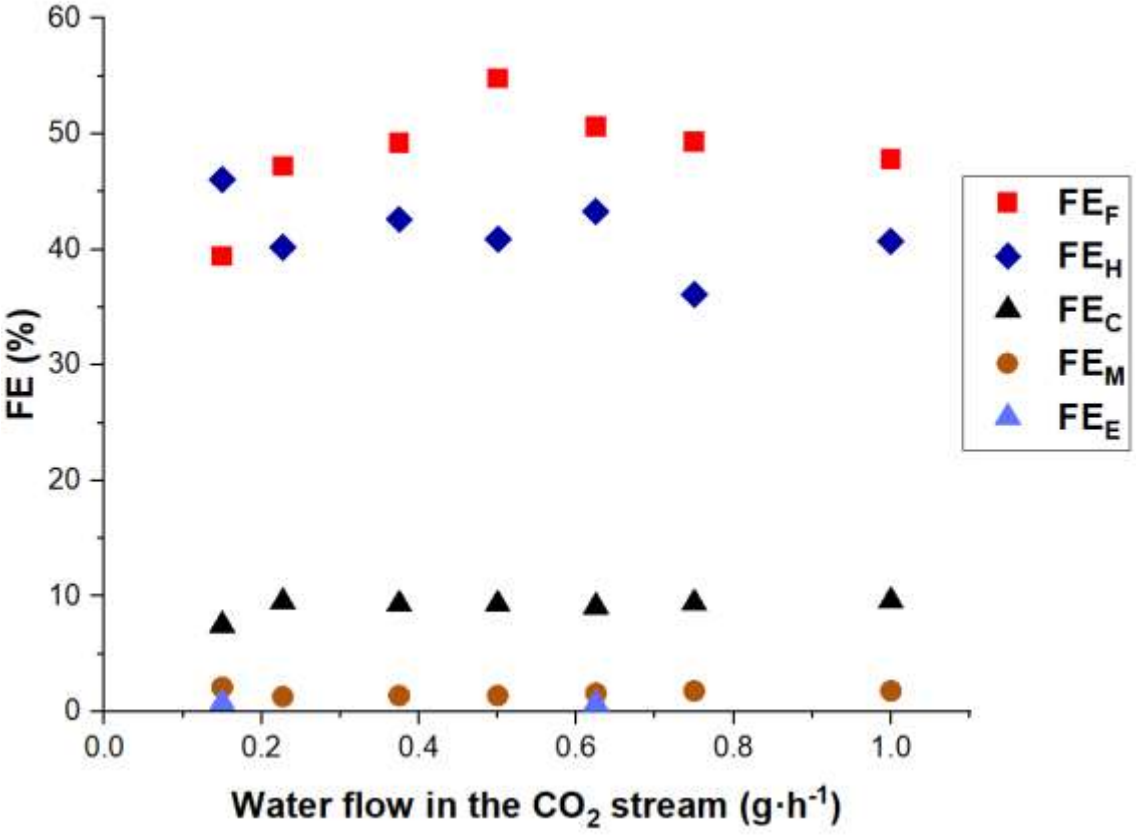


**Fig. 8.** Influence of water input flow in the $CO_2$ stream on *FE* to formate ($FE_F$), hydrogen ($FE_H$), carbon monoxide ($FE_C$), methane ($FE_M$), and ethylene ($FE_E$) in the water flow range of 0.15–1 $g \cdot h^{-1}$ applied at constant current density = 45 $mA \cdot cm^{-2}$, Bi *CL* = 0.75 $mg \cdot cm^{-2}$, as measured at room temperature.

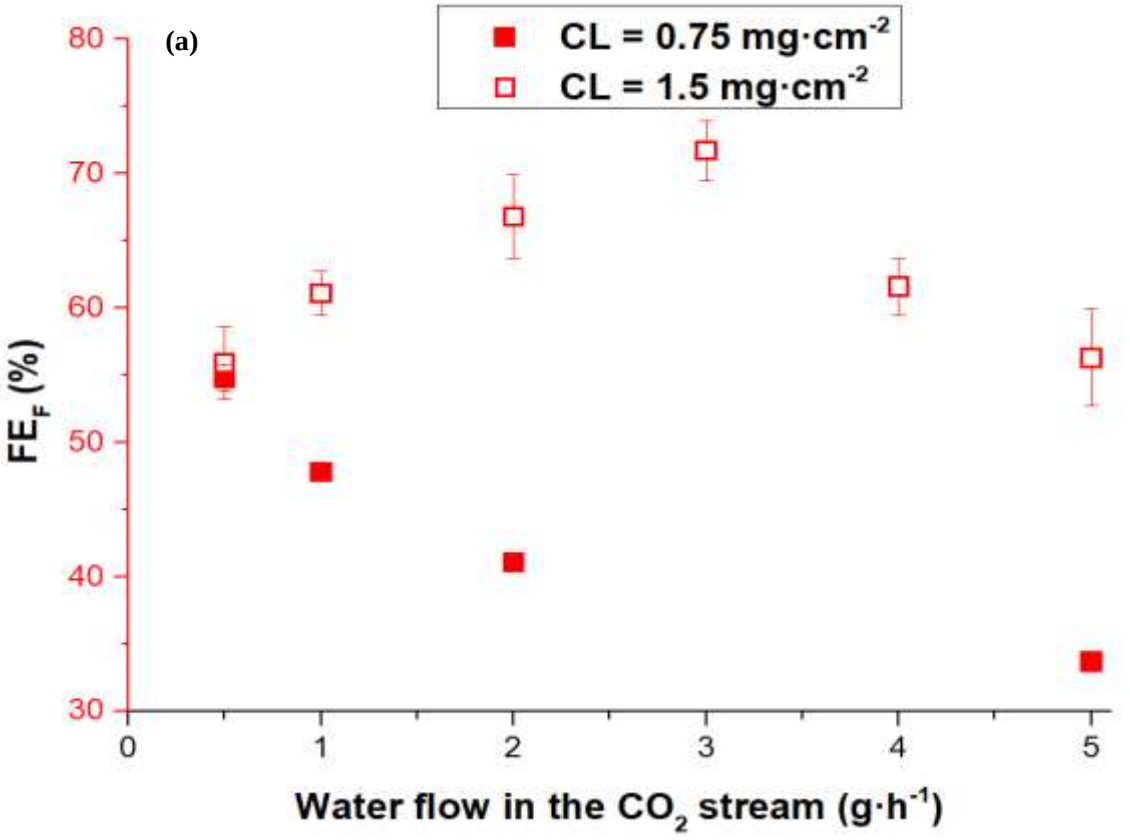


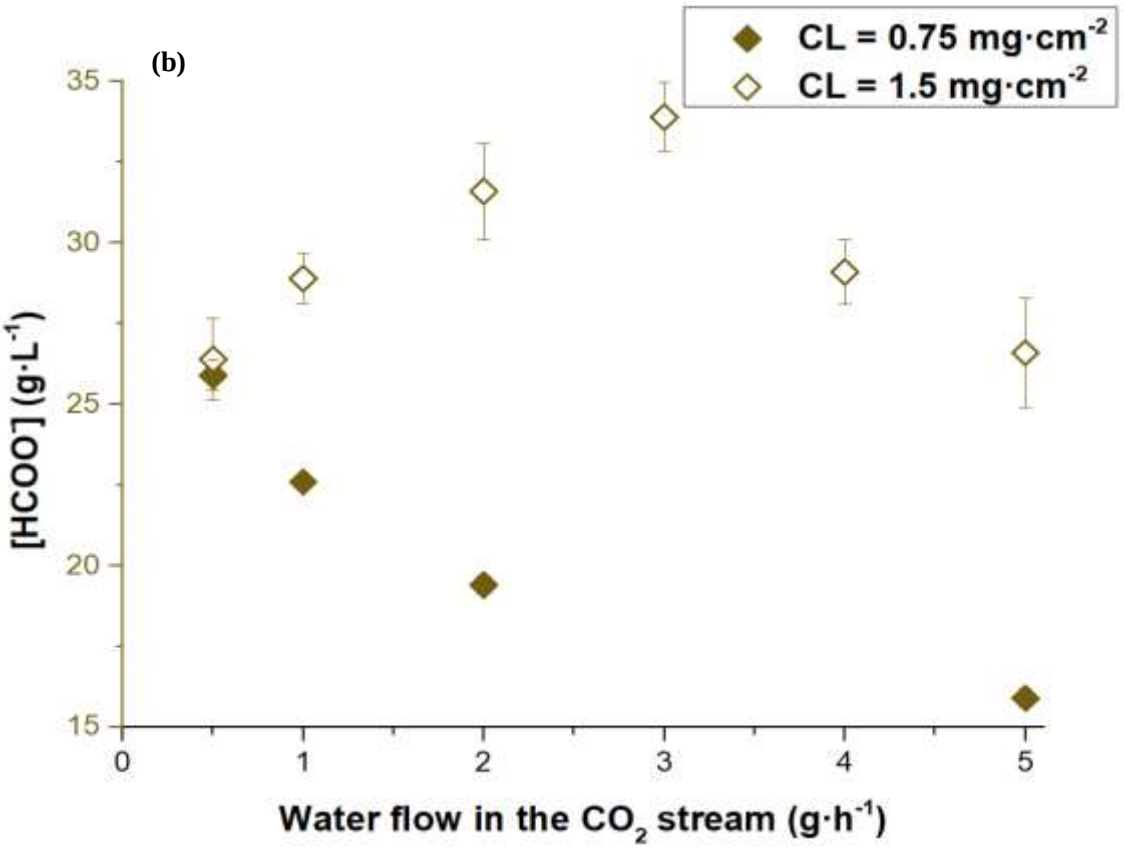

**Fig. 9.** Influence of water flow in the $CO_2$ stream on (a) Faradaic efficiency for formate (%) and (b) formate concentration ($g \cdot L^{-1}$) working with Bi/C-CCMEs with a Bi *CL* = 0.75 $mg \cdot cm^{-2}$ and 1.5 $mg \cdot cm^{-2}$ in the water flow range of 0.5–5 $g \cdot h^{-1}$ at a constant current density of 45 $mA \cdot cm^{-2}$ as measured at room temperature.

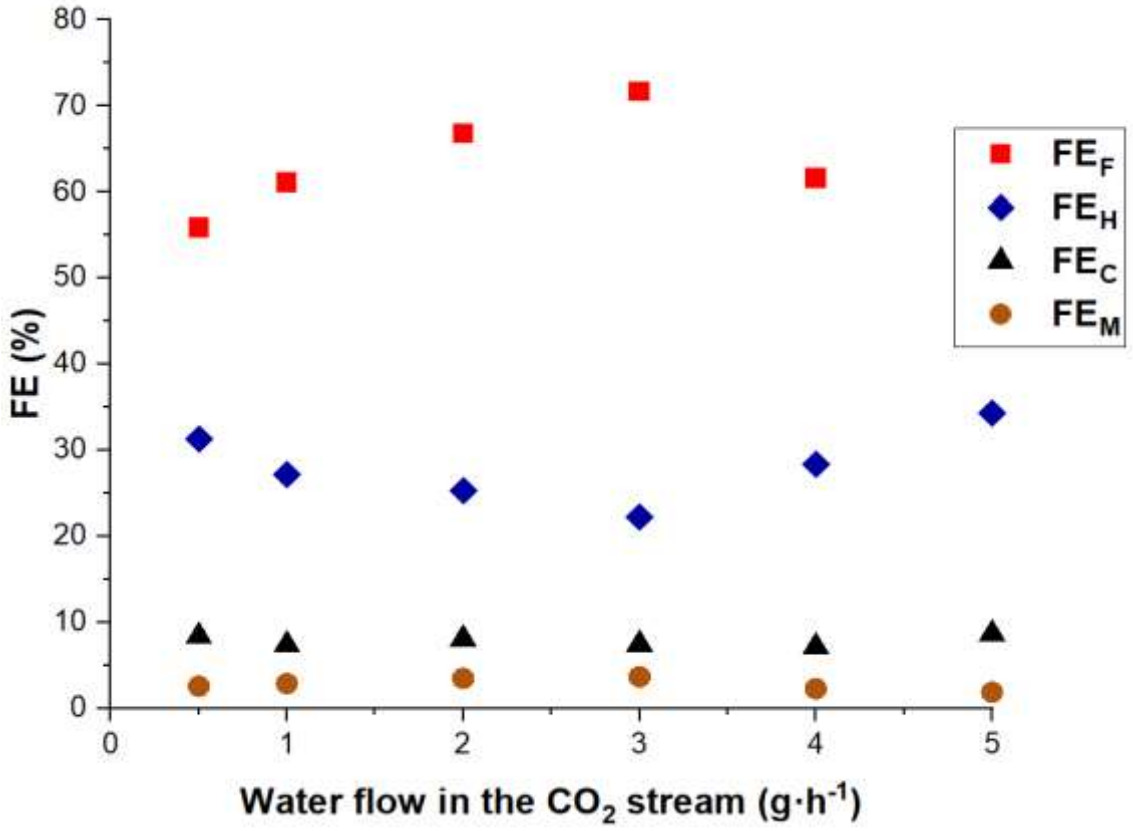


**Fig. 10.** Influence of water input flow in the $CO_2$ stream on FE to formate ($FE_F$), hydrogen ($FE_H$), carbon monoxide ($FE_C$), and methane ($FE_M$) working with Bi/C-CCMEs with a Bi *CL* = 1.5 mg·cm$^{-2}$ in the water flow range of 0.5–5 g·h$^{-1}$ applied at a constant current density of 45 mA·cm$^{-2}$, as measured at room temperature.

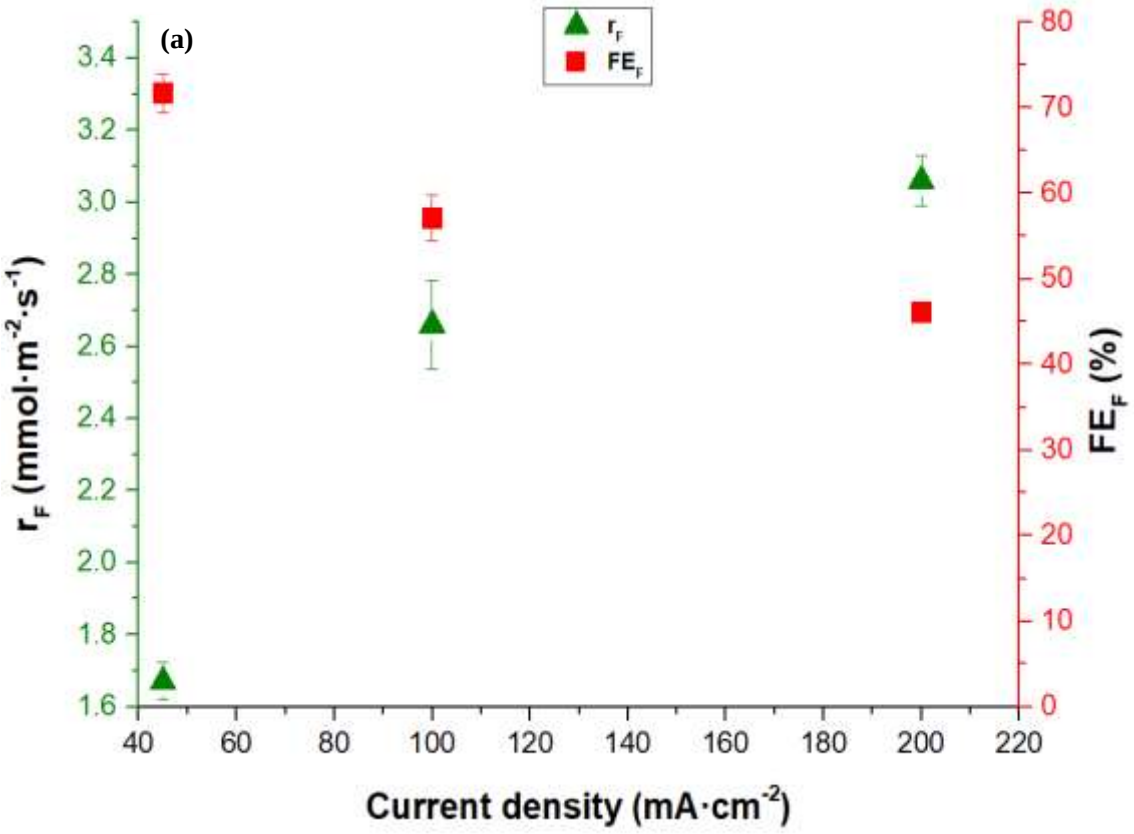


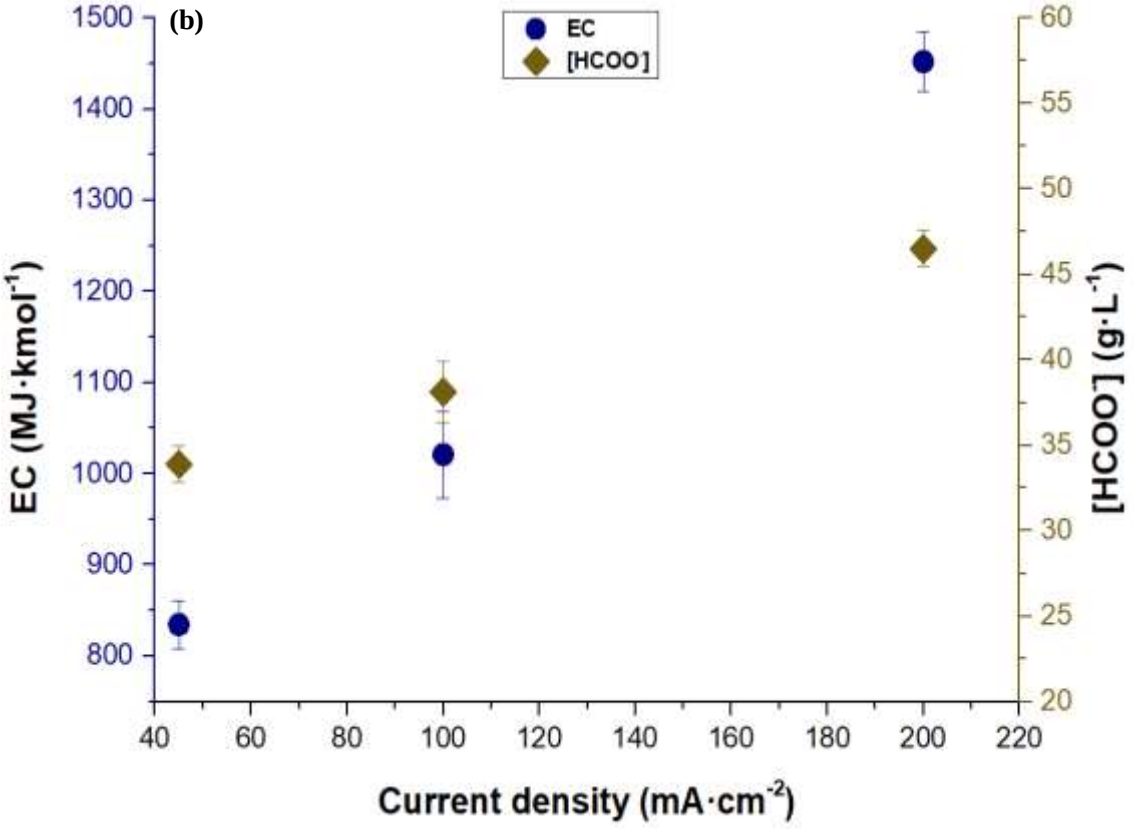

**Fig. 11.** Influence of current density on (a) formate rate (mmol·$m^{-2}$·$s^{-1}$) and Faradaic efficiency for formate (%) and (b) consumption of energy per kmol of formate (MJ·$kmol^{-1}$) and formate concentration (g·$L^{-1}$) in the current density range of 45–200 mA·$cm^{-2}$ operating at 293 K, Bi *CL* = 1.5 mg·$cm^{-2}$, and water flow in the $CO_2$ stream = 3 g·$h^{-1}$.